

Quantum-dot-based Kitaev chains: Majorana quality measures and scaling with increasing chain length

Viktor Svensson and Martin Leijnse

Division of Solid State Physics and NanoLund, Lund University, S-221 00 Lund, Sweden

(Dated: December 6, 2024)

Realizing Majorana bound states (MBSs) in short, well-controllable chains of coupled quantum dots sidesteps the problem of disorder, but requires fine-tuning and does not give the true topological protection inherent to long chains. Here, we introduce a new quality measure that is applicable also in the presence of strong electron-electron interactions and that quantifies the closeness to topological protection of finetuned MBSs in short quantum-dot chains. We call this measure local distinguishability because it puts a bound to the degree an arbitrary local measurement can distinguish between two states. We study the local distinguishability for quantum-dot chains of different length. The three-dot chain is studied in detail, and we find that it may not always be an improvement over the two-dot case, a fact that can be understood within an effective model derived from perturbation theory. For longer chains, the local distinguishability vanishes exponentially, signalling a transition to a topological phase with two ground states that cannot be distinguished by any local measurement.

I. INTRODUCTION

The past 15 years have seen a surge of efforts aiming to realize the physics of the so-called Kitaev chain [1], which features a topological superconducting phase. This phase is associated with Majorana bound states (MBSs), zero energy excitations with non-abelian statistics [2–6] that could be used for topological quantum computation [7–9]. Many different systems can be engineered to have a low-energy subspace that realizes an effective Kitaev chain, including, for example, proximitized nanowires [10–15], magnetic adatoms [16, 17], and planar Josephson junctions [18–21]. However, the disorder present in all these platforms complicates the realization and experimental detection of a topological superconducting phase and MBSs [22–33].

Because of this, the proposal to implement a Kitaev chain in well-controllable coupled quantum dots [34–36] has attracted increasing attention. Device complexity increases with more dots and short chains are preferable, but fortunately already the two-dot chain can host MBSs [35]. The price to pay in short chains is that there is no true topological phase – the system must be fine-tuned to a *sweet spot* to show signatures of MBSs and some protection against perturbations. Because of the lack of formal topological protection, the associated states have been called poor man’s MBSs. Various new ideas for how to design and tune such two-dot chains have been explored theoretically [37–41], and experimentally realized [42–45].

Experimentally distinguishing MBSs from topologically trivial Andreev bound states has proven to be a difficult problem. Experiments on the quantum-dot platform [43–45] have already demonstrated correlated appearance and splittings of zero-bias peaks at both ends of the chain, as well as signatures in the nonlocal conductance that are consistent with (poor man’s) MBSs. Conductance measurements in a setup including an additional probe quantum dot could provide additional es-

timates of the nonlocal properties of the wavefunction [46]. However, making conclusive statement about the closeness of the observed states to true topological MBSs would require protocols aimed at demonstrating non-abelian physics [47–49]. It is also an interesting theoretical problem to define a MBS quality measure, that quantifies the similarity of a given state to a true topological MBS. One such measure that is based on the MBS wavefunction is the Majorana polarization (MP) [38, 50–52]. However, in the presence of electron-electron interactions, which are typically very strong in the quantum-dot platform, the many-body nature of the MBSs [53–59] complicates the interpretation of the MP.

In this article, we introduce a MBS quality measure based on the local distinguishability of ground states in topological phases, which has no extra difficulty in interacting systems and gives a rigorous bound on the protection against perturbations. Increasing the length of the system should produce better quality MBSs, and recent experimental results on a three-dot Kitaev chain [60, 61] shows an increased stability of the energy spectrum under certain perturbations. There is also recent theoretical work on scaling up to longer length chains [62, 63]. Here, we analyze the protection as a function of the chain length, paying particular attention to the three-dot case. We find that the protection in this case may be *worse* in some respects than the two-dot case, and we explain these results with an effective Hamiltonian derived by perturbation theory.

The paper is organized as follows: Section II describes the system and Section III discusses how to characterize and quantify the quality of MBSs and how to tune a system to a sweet spot in parameter space where such quality measures are maximized. Section IV A then focuses on how to tune the three-dot chain and shows that it can be worse than the two-dot chain in some respects, while Section IV B contains a derivation of an effective model to explain these results. Finally, Section IV C shows what happens when scaling to longer chains.

II. SYSTEM

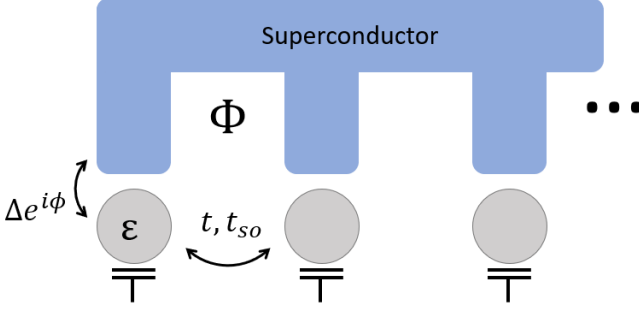


FIG. 1. Sketch of setup where each quantum dot is coupled to the bulk superconductor via a local proximity effect (with amplitude Δ and phase ϕ), and to its neighbours via both spin-preserving and -flipping tunneling (with amplitudes t and t_{so}). The dot levels ε and magnetic flux Φ (controlling the phase ϕ) are used to tune to a sweet spot.

The system we consider consists of a chain of quantum dots, each locally coupled to a superconductor and coupled to each other via tunneling, see Fig. 1. This setup was proposed in Ref. [36] and the two-dot interacting version was studied in detail in Ref. [40], where it was shown that for a wide range of parameters it exhibits a sweet spot with localized MBSs, which can be reached by tuning the dot levels ε_j and the superconducting phases ϕ_j (controlled by the magnetic fluxes Φ_j through the loops). As $V_Z, \Delta \rightarrow \infty$, the system reduces to a Kitaev chain.

The system Hamiltonian consists of two parts,

$$H = H^{\text{QD}} + H^C, \quad (1)$$

where H^{QD} contains all the terms local to each of the N dots and H^C contains the coupling between them. These parts take the form

$$H^{\text{QD}} = \sum_{j=1}^N \sum_{\sigma} (\varepsilon_j + \eta_{\sigma} V_{Z,j}) n_{j\sigma} + (\Delta_j e^{i\phi_j} d_{j\uparrow}^{\dagger} d_{j\downarrow}^{\dagger} + \text{h.c.}) + U_{l,j} n_{j\uparrow} n_{j\downarrow} \quad (2a)$$

$$H^C = \sum_{j=1}^{N-1} \sum_{\sigma} (t_j d_{j\sigma}^{\dagger} d_{j+1\sigma} + \text{h.c.}) + (\eta_{\sigma} t_{so,j} d_{j\sigma}^{\dagger} d_{j+1\bar{\sigma}} + \text{h.c.}) + U_{nl,j} N_j N_{j+1}, \quad (2b)$$

where $d_{j\sigma}^{\dagger}$ creates an electron with spin σ on dot j , $n_{j\sigma} = d_{j\sigma}^{\dagger} d_{j\sigma}$, $N_j = n_{j\uparrow} + n_{j\downarrow}$ and $\eta_{\sigma} = \pm$. The local term includes the dot levels ε_j , Zeeman splitting V_Z , induced local pairing Δ_j and its phase ϕ_j , and the local Coulomb interaction $U_{l,j}$. The term coupling dots together includes spin-conserving and spin-flip tunnelling t_j and $t_{so,j}$, and the non-local Coulomb interaction $U_{nl,j}$.

III. PROTECTION AND SWEET SPOT QUALITY

In this section, we discuss how to characterize the kind of protection implied by the existence of MBSs, the essential differences between short and long chains, and define how we search for a sweet spot. We denote by $|o\rangle$ and $|e\rangle$ the ground states in the odd and even fermionic parity sectors respectively and define $\delta\rho = |o\rangle\langle o| - |e\rangle\langle e|$. Their energy difference is δE and E_{ex} is the gap to excited states.

The existence of non-overlapping Majorana operators implies that the two ground states can't be distinguished by *any* local measurement. Local means here that the spatial size of the terms in the operator is smaller than the separation between the MBSs. In particular, if the Hamiltonian is local, then $\delta E = 0$. This is the case for a long Kitaev chain in the topological phase. This degeneracy is stable under any local perturbation \mathcal{O} as

$$\begin{aligned} \delta E &= \langle H + \mathcal{O} \rangle_o - \langle H + \mathcal{O} \rangle_e \\ &= \text{Tr}[\mathcal{O} \delta\rho] \end{aligned} \quad (3)$$

corresponds to the difference of a local measurement of the states. Characterizing the quantity $\text{Tr}[\mathcal{O} \delta\rho]$ will be one of the main points of this article.

In short chains, even non-overlapping MBSs may be close enough to be coupled together by the Hamiltonian. The Hamiltonian is in this sense *non-local* and δE may be non-zero even if the MBSs are perfectly localized to the edges. This splitting introduces an undesirable dynamical phase in fusion and braiding protocols. For a non-local Hamiltonian, $\delta E = 0$ is an independent condition from the separation of MBSs. Therefore, as we search for the sweet spot, we will consider these independently.

A. Protection from fluctuating parameters

The stability of δE is not necessarily related to the presence of separated MBSs. Consider a Hamiltonian $H(\lambda)$ that is a function of some parameter λ . Protection against fluctuations in λ may arise in several ways, some of which are

1. $\left\| \frac{\partial H}{\partial \lambda} \delta\lambda \right\|$ is small because the Hamiltonian is naturally insensitive to variations in λ .
2. $\text{Tr}[\delta\rho \frac{\partial H}{\partial \lambda}]$ is small, because $\delta\rho$ is orthogonal to this particular perturbation.
3. There are non-overlapping MBSs that map between the ground states and the Hamiltonian is local.

The first type has nothing to do with MBSs. The second type is implied by the third, but can also occur when the MBSs overlap, see Sec. IV A 1. The third type is the strongest and implies protection based only on the *locality* of the perturbations and the MBS wavefunction.

B. Majorana Polarization

In non-interacting systems the MBS wavefunction is simple to define and the Majorana polarization (MP) can be used to characterize how separated the two MBSs are [50, 51]. A generalization has been used in interacting systems [38, 40, 52] but in this case it cannot fully characterize MBSs with non-trivial many-body content [54–58]. We use the definition from Ref. [40],

$$\text{MP} = \frac{\left| \sum_{l,s} \langle e | \gamma_{ls} | o \rangle^2 \right|}{\sum_{l,s} \left| \langle e | \gamma_{ls} | o \rangle^2 \right|}, \quad (4)$$

where $|o\rangle$ and $|e\rangle$ are the odd and even ground states, l indexes the fermions on the leftmost site [64] and

$$\gamma_{l+} = d_l + d_l^\dagger, \quad (5a)$$

$$\gamma_{l-} = i(d_l - d_l^\dagger). \quad (5b)$$

We have chosen to focus on the outer dots, and by reflection symmetry, we don't need to consider the rightmost dot. For a non-interacting system, $\text{MP} = 1$ implies that there is no overlap of the MBSs on the outer dots and the system is protected from perturbations at those dots. However, with interactions, or imperfect MP, there is no clear quantitative relation between the MP and protection from perturbations.

C. Local distinguishability

Due to the difficulties with the MBS wavefunction, we introduce a measure based on the local distinguishability of the ground states. This measure provides a rigorous bound on the stability of δE and is well-defined even with interactions. Our construction is inspired by Ref. [56] where the presence of MBSs is diagnosed by probing the ground states with local measurements such as the charge on each dot. We extend this to cover *all* local measurements.

Consider a perturbation \mathcal{O}_R acting only in some subsystem R . The rest of the system is denoted by the complement R^c . To first order in this perturbation, the energy difference between the ground states changes if the perturbation can distinguish the states, see Eq. 3. This quantity obeys

$$|\text{Tr}[\mathcal{O}_R \delta \rho]| = |\text{Tr}[\mathcal{O}_R \delta \rho_R]| \leq \|\mathcal{O}_R\| \|\delta \rho_R\| \quad (6)$$

where $\delta \rho_R = \text{Tr}_{R^c} \delta \rho$ is the difference in reduced density matrices and $\|\cdot\|$ is the Frobenius norm [65]. We see that $\|\delta \rho_R\|$ bounds the effect of any perturbation in the region R . In App. A we show that it is zero if there exists a MBS outside of the region R .

In a topological phase, $\|\delta \rho_R\| = 0$ in all sufficiently local regions. For our system, we take the subsystems to

be each individual dot, and define the local distinguishability (LD) as

$$\text{LD} = \sqrt{\sum_i \|\delta \rho_{Q_{D_i}}\|^2} \quad (7)$$

which we minimize when optimizing for the sweet spot.

LD is simple to compute as it only relies on finding ground states. It can be calculated in large interacting systems by using e.g. DMRG. In non-interacting systems, the reduced density matrix can be reconstructed from the single particle density matrix.

D. Optimizing for a sweet spot

In this section, we define how we optimize for sweet spots, both with and without energy degeneracy and introduce notation to keep the different cases apart. The term sweet spot is used interchangeably for all of them.

We denote by mLD_0 the minimal LD point with degenerate ground states, i.e. the solution to the minimization problem

$$\begin{aligned} \min \quad & \text{LD} \\ \text{s.t.} \quad & \delta E = 0. \end{aligned} \quad (8)$$

In practice, we impose the latter condition by solving the problem

$$\min \quad \text{LD} + \lambda |\delta E| \quad (9)$$

which includes a penalty factor λ that enforces the constraint. We will compare this point to the point denoted by mLD , defined by the solution to

$$\min \quad \text{LD},$$

which does not require the states to be degenerate.

Another approach to defining a sweet spot, used in e.g. Refs. [41, 59], is to optimize for a spot with degenerate ground states and where that degeneracy is protected against fluctuations in the dot levels ε . In other words, where $\frac{\partial \delta E}{\partial \varepsilon} = 0$. We call this the level-protected point. Since we also tune the phase difference $\delta \phi$, we also consider a phase-protected point defined analogously. These points are in general different from the mLD points.

IV. RESULTS

We start by analyzing the three-dot case in Sec. IV A, comparing the different sweet spots in detail. The observations will be explained with perturbation theory in Sec. IV B, and in Sec. IV C we consider longer chain lengths. Our results are produced with the code available at [66].

The constant parameters are set to

$$t_{\text{so}}/t = 5 \quad (10a)$$

$$\sqrt{t^2 + t_{\text{so}}^2} = \Delta/2 \quad (10b)$$

$$V_Z = 3\Delta. \quad (10c)$$

When $t > t_{\text{so}}$, it is advantageous to tune ε in an alternating manner to effectively enhance the spin-flipping process [40]. Picking $t < t_{\text{so}}$ is simpler, because the sweet spot is closer to homogeneous. Similar results are expected in both cases as the effective Hamiltonians (see Sec.IV B and App.D) are the same at first order in perturbation theory.

For simplicity we also set

$$U_l = U_{\text{nl}} = 0 \quad (11)$$

for the results in the main paper as we found that the essential features we focus on in this work are qualitatively the same with and without Coulomb interactions. The main thing to keep in mind is that there is a limit to how large interaction strengths can be tolerated, see App.C for details.

A. Three-dot system

In this section we consider a three-dot system and how to tune it to a sweet spot. Assuming reflection symmetry, we have three independent parameters to tune, $\varepsilon_1 = \varepsilon_3 = \varepsilon$, ε_2 , $\delta\phi = \phi_2 - \phi_1 = \phi_3 - \phi_2$. In Sec.IV A 1, we reduce it to two parameters by setting $\varepsilon_1 = \varepsilon_2$, making it easy to visualize. In Sec.IV A 2 we study how the sweet spot can be improved by tuning ε_2 independently.

1. Homogeneous tuning

We start with a three-dot system where we tune the dot levels ε and phase gradient $\delta\phi$ homogeneously. The heatmap in Fig.2 shows LD as these parameters are tuned, and the contour lines show the energy splitting between the two ground states. Unfortunately, and differently from the two-dot case, the solid lines where the ground states are degenerate do not lie in the region with well separated MBSs and good protection.

In Fig. 2, the condition $\delta E = 0$ is satisfied on the solid contour lines, which has two disconnected branches. One branch features a point where it the contour is tangent to the horizontal axis. At this point, the degeneracy is protected from variations in ε . We call this the level branch. The other branch is called the phase branch as it features a point tangent to the vertical axis with protection against phase fluctuations. These tangential points feature protection against a specific perturbation, an example of type 2 protection as defined in Sec.III.

On each branch, we can also define a point with minimal LD and $\delta E = 0$, denoted by mLD₀ and marked in

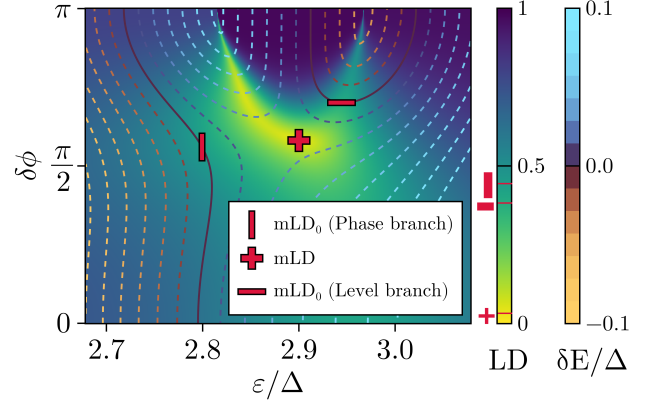


FIG. 2. Tuning ε and $\delta\phi$ homogeneously in the three-dot chain. Brighter color means a smaller LD. The contours show the energy splitting between ground states δE , with solid line signifying degeneracy. The three points marked are defined in Sec.III D, and correspond to points with minimal LD, with and without energy degeneracy.

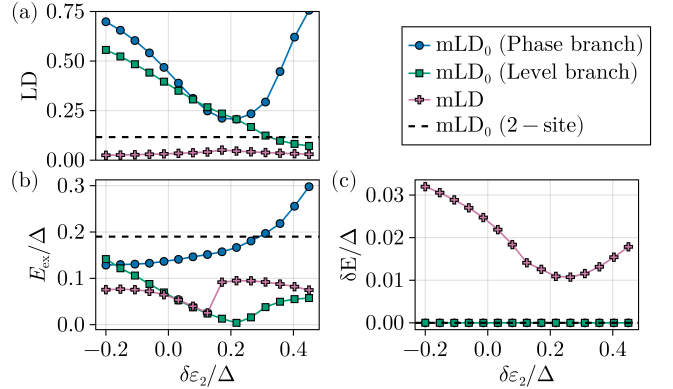


FIG. 3. Sweet spot properties as a function of the middle dot detuning $\delta\varepsilon_2$. The mLD₀ points on the two branches improve, but can't clearly beat the two-dot sweet spot without reducing the excitation gap. As the detuning increases, the phase branch becomes irrelevant while the level branch should be thought of as an effective two-dot chain where the middle dot acts as a tunnel barrier. At $\delta\varepsilon_2 \approx \Delta/5$, the location of the mLD point changes location discontinuously, see App. B.

the figure. These differ from the tangential points, but on the level branch they are very close. The constraint of $\delta E = 0$ severely limits the quality of the sweet spot. The point marked + and denoted by mLD has a non-zero δE but LD is much smaller. Here, there are well-separated MBSs and the energy splitting is to some degree protected against *any* local perturbation, but the ground states are not degenerate. We will see why in Sec.IV B.

2. Inhomogeneous tuning

Fig. 2 shows that there is a tension between energy degeneracy and good MBSs at the sweet spot. Here, we check that this is still the case even if the system is tuned inhomogeneously. We detune the middle dot so that $\varepsilon_2 = \varepsilon + \delta\varepsilon_2$.

In Fig. 3, we follow the phase branch and level branch of the sweet spot as a function of the detuning $\delta\varepsilon_2$. The sweet spots improve, especially the phase branch which reaches an LD and excitation gap comparable to the two-dot case. When the detuning gets large enough, the phase branch quickly gets worse, while the level branch features a small LD but with a bad excitation gap. Effectively, the middle dot has been detuned to act as a tunnel barrier and the three-dot chain can be effectively reduced to a two-dot chain. We conclude that the three-dot chain does not improve on the two-dot chain in this way of measuring the protection. Note that our definition of LD does not cover all possible perturbations, only those local to each dot. It also only quantifies first order protection, and says nothing about higher order terms.

B. Effective model

The three-dot chain seems to offer a *worse* protection against local perturbations than the two-dot chain when we impose energy degeneracy. In this section we show why, by deriving an effective model to second order in t/V_Z . The second order terms give a Kitaev chain that includes next-nearest neighbours hoppings and pairings. This makes the effective Hamiltonian less local, and it can then more easily distinguish the ground states.

1. Deriving the effective model

We can derive an effective Kitaev model using perturbation theory. We follow [36, 40] and treat the hopping as a perturbation of H^{QD} . We first transform $d_n \rightarrow d_n e^{i\phi_n/2}$ to put the phase winding on the hopping. H^{QD} is diagonalized by a Bogoliubov transformation

$$d_{n\downarrow}^\dagger = \frac{\sqrt{\beta_n - \epsilon_n} a_n^\dagger - \sqrt{\beta_n + \epsilon_n} b_n^\dagger}{\sqrt{2\beta_n}} \quad (12a)$$

$$d_{n\uparrow}^\dagger = \frac{\sqrt{\beta_n + \epsilon_n} a_n^\dagger + \sqrt{\beta_n - \epsilon_n} b_n^\dagger}{\sqrt{2\beta_n}} \quad (12b)$$

where $\beta_j = \sqrt{\varepsilon_j^2 + \Delta_j^2}$. The a and b fermions have energies

$$E_{a_j} = \beta_j - V_Z,$$

$$E_{b_j} = \beta_j + V_Z,$$

and we consider the regime where $E_a \ll E_b$ and integrate out the b -fermions. Let P be the projector on the subspace with no occupied b -fermions, and $Q = I - P$. To

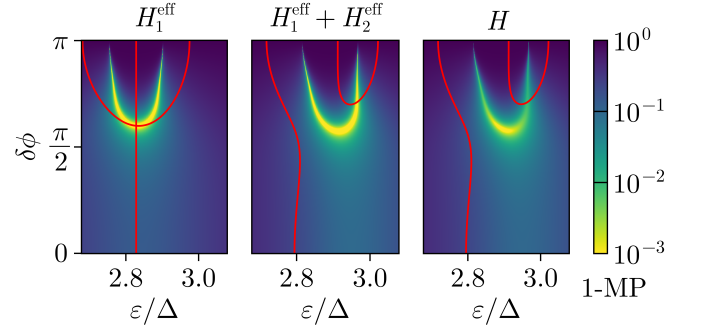


FIG. 4. The heatmap shows the MP (see Eq. 4) and the red contour shows where the ground states are degenerate. The first order effective Hamiltonian has a sweet spot where MP is maximized and the two branches of $\delta E = 0$ coincide. In the second order model (which closely resembles the full model), the $\delta E = 0$ lines do not coincide with the maximum in MP. This is due to the additional long range couplings which can be significant if the Zeeman splitting is finite.

second order in the hoppings, the effective Hamiltonian in the subspace P is

$$\begin{aligned} H^{\text{eff}} &= PHP - \frac{1}{2E_b} PH^C QH^C P \\ &= H_1^{\text{eff}} + H_2^{\text{eff}}. \end{aligned} \quad (13)$$

The b -fermions have been integrated out, but leave a trace in the form of the second order term.

The first term is a standard Kitaev chain,

$$H_1^{\text{eff}} = \sum_n \varepsilon_a a_n^\dagger a_n + (t_{aa} a_n^\dagger a_{n+1} + \Delta_{aa} a_n a_{n+1} + \text{h.c.}) \quad (14)$$

as derived previously for this model in [36, 40]. The explicit expressions for the parameters for a homogeneous system are shown in App. D. The second term,

$$H_2^{\text{eff}} = \sum_n \varepsilon_2 a_n^\dagger a_n + t_2 a_n^\dagger a_{n+2} + \Delta_2 a_n^\dagger a_{n+2} + \text{h.c.}, \quad (15)$$

includes longer range terms that couple next nearest neighbours. This is not unique to this system, the same thing happens in other dot-based Kitaev chains [67]. Kitaev chains with long range couplings have been studied in Refs. [68–70]. These terms are to blame for the complications of the three-dot sweet spot, as they make the Hamiltonian more non-local.

We confirm this with Fig. 4. It shows the tuning plot, now for the MP for the first and second order effective Hamiltonian, and for the full model. The first order effective model, which corresponds to a standard Kitaev chain, has a definitive sweet spot where the ground states are degenerate, $\text{MP} = 1$ and $\text{LD} = 0$. The two branches where $\delta E = 0$ cross at the sweet spot and the contours are tangential to both axes. When the longer range terms of H_2^{eff} are included, the plot closely resembles the result of the full model, where the branches avoid each other as

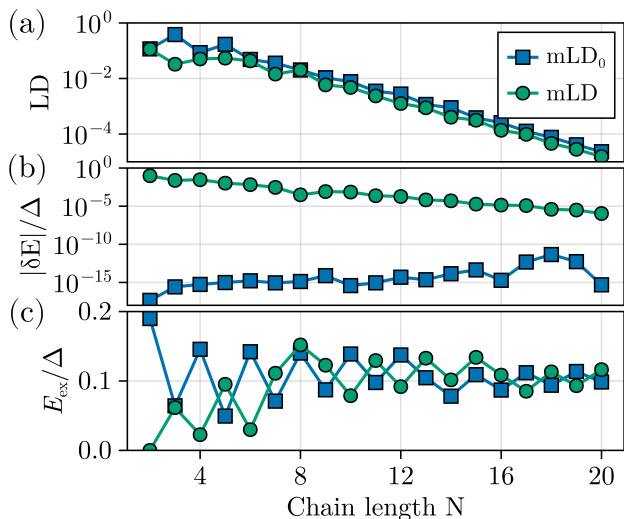


FIG. 5. Sweet spot quality as a function of chain length with homogeneous tuning. (a) LD has an exponential fall-off at large chain lengths, implying exponentially better protection. At small lengths, the pattern is less clear. (b) The energy splitting δE . (c) The excitation gap is somewhat stable around $E_{\text{ex}} \sim \Delta/10$ for long chains. For $N = 2$ and 4, the excitation gap at mLD is very small, with only a very small improvement in LD over mLD₀.

well as the point with maximally separated MBSs. Comparing Figs. 2 and 4 we also see that the two measures of sweet spot quality, MP and LD, are correlated.

C. Scaling to longer chains

In this section, we optimize homogeneously over dot levels and phase differences to find the sweet spot as a function of the length of the chain. At large system sizes, exact diagonalization of the many body Hamiltonian is prohibitively expensive, but since we consider a non-interacting theory at this point, the reduced density matrices ρ_{QD_i} on each dot can be reconstructed from the correlators $\langle c_i^\dagger c_j \rangle$ and $\langle c_i^\dagger c_j^\dagger \rangle$ [71, 72] which are obtainable via standard Bogoliubov-de-Gennes techniques.

As seen in Fig. 5(a), LD at the sweet spot falls off exponentially as the chain length increases. This is expected in a topological phase. Fig. 5(b) shows the splitting of the ground state degeneracy δE , which is constrained to be very small for mLD₀. At the point mLD, there is no constraint on the energy splitting, but since LD falls off exponentially, one would expect δE to follow the same pattern. Fig. 5(c) shows the excitation gap at the sweet spot, which has an odd-even pattern but is otherwise quite stable at $E_{\text{ex}} \sim \Delta/10$.

Fig. 6(a) shows the tuning diagram for a 40-dot chain, where a phase diagram starts taking shape. For long enough chains, any point in the topological phase has good protection and energy degeneracy and there is no

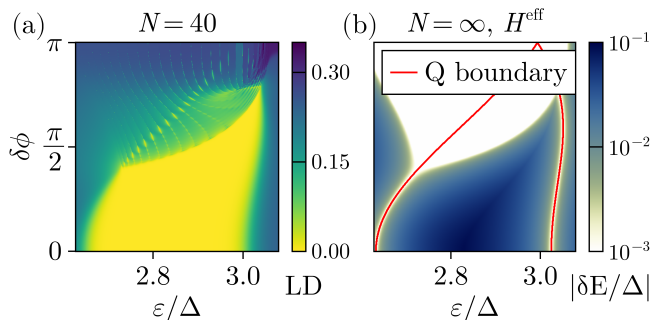


FIG. 6. Phase diagrams for finite and infinite systems. (a) In an open system with 40 sites LD shows clear phase boundaries. (b) In an infinite, periodic system, with the second order effective Hamiltonian, there is a topological phase and a trivial phase separated by the red contour where the topological invariant changes sign and the gap closes at $k = 0$ or $k = \pi$. The heatmap shows the energy gap which also reveals an extended region where the gap closes at a finite momentum.

need to fine-tune to a sweet spot. The patterns seen in Fig. 6(a) can be matched with the true phase diagram of the infinite system in 6(b). Since the second order effective model captures the physics well, we use it to determine a topological invariant Q (see App. E) that signifies when the gap closes at $k = 0$ or $k = \pi$. It can take on the values $+1$ (trivial phase) or -1 (topological phase) and the boundary between these is plotted as the red contour in Fig. 6(b). Due to the breaking of time reversal symmetry, there is also a gapless phase where the gap closes at finite momentum [68], which can be seen in the heatmap of Fig. 6(b) that shows the energy gap of the infinite, periodic system.

V. SUMMARY AND CONCLUSIONS

In this work, we have introduced the local distinguishability of ground states as a quality measure of near-topological phases in finite and (possibly) strongly interacting systems, and applied this measure to quantum-dot-based Kitaev chains of varying length. It has a clear experimental signature in that it bounds the energy splitting of any local perturbation. Conversely, local measurements provide lower bounds on LD, but determining the actual value requires in general performing *all* local measurements.

As expected, the local distinguishability decreases exponentially for long chains indicating a transition to a true topological phase, but for short chains the pattern is different. In particular, we have shown that the three-dot case can actually be worse than the two-dot case. The explanation for this result is that the long-range nature of the effective Hamiltonian introduces a trade-off between separated MBSs and the energy degeneracy between the ground states. This has consequences for

protocols aiming to demonstrate the non-abelian nature of MBSs, which rely on both energy degeneracy and the MBSs not overlapping [49]. It would be an interesting direction for future works to investigate if non-abelian protocols can be designed that only require the ground state energy splitting to be *stable*, not zero. On a more general level, much remains to be understood concerning the topological-like protection and nonabelian properties of strongly interacting, finite systems.

ACKNOWLEDGMENTS

We acknowledge stimulating discussions with Chun-Xiao Liu, William Samuelson, Michael Wimmer and Mert Bozkurt and funding from the European Research Council (ERC) under the European Unions Horizon 2020 research and innovation programme under Grant Agreement No. 856526, the Swedish Research Council under Grant Agreement No. 2020-03412, and NanoLund.

Appendix A: Local Distinguishability and MBSs

Here, we show that $\|\delta\rho_R\| = 0$ if there exists a Majorana operator in the complement. If there exists a Hermitian operator $\gamma = I_R \otimes \gamma_{R^c}$ such that $|e\rangle = \gamma|o\rangle$ and $\gamma_{R^c}^2 = I$, then by the cyclic property of the partial trace

$$\text{Tr}_{R^c} |e\rangle\langle e| = \text{Tr}_{R^c} [\gamma_{R^c} |o\rangle\langle o| \gamma_{R^c}] = \text{Tr}_{R^c} |o\rangle\langle o| \quad (\text{A1})$$

and therefore $\delta\rho_R = 0$. This is a necessary condition for the existence of MBSs outside of R , but not sufficient.

If there are several such operators, then $\delta\rho_R$ can only be non-zero in regions that include all of them, as it vanishes if any one of them is outside R .

Appendix B: More on branches

In Fig. 7 some additional plots for the three-dot chain as a function of the detuning of the middle dot, complementing Fig 3.

We plot the gradient of the ground state energy splitting $\|\nabla\delta E\|$ in Fig. 7(a), where $\nabla \equiv \left[\frac{\partial}{\partial \varepsilon} \quad \frac{\partial}{\partial \phi} \right]$. Note that we still optimize for a minimal LD, not for minimal gradient. The gradient differs somewhat from the LD since it is sensitive to details such as how the Hamiltonian is parameterized. In other words, it also includes the effect of type 1 and 2 protection as explained in Sec. III. The location of the sweet spots is shown in Figures 7(b) and (c), where we see that the mLD_0 points on the level and phase branch can be followed continuously while the mLD has a discontinuous jump.

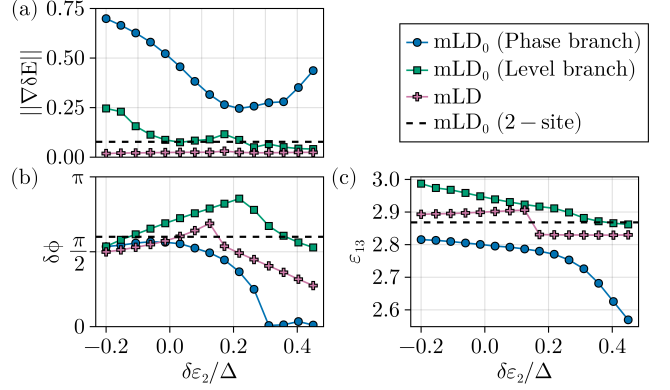


FIG. 7. Similar to Fig. 3, we follow different sweet spots as a function of the detuning $\delta\varepsilon_2$. (a) norm of the gradient of δE . (b) $\delta\phi$ at the sweet spot. (c) ε at the sweet spot.

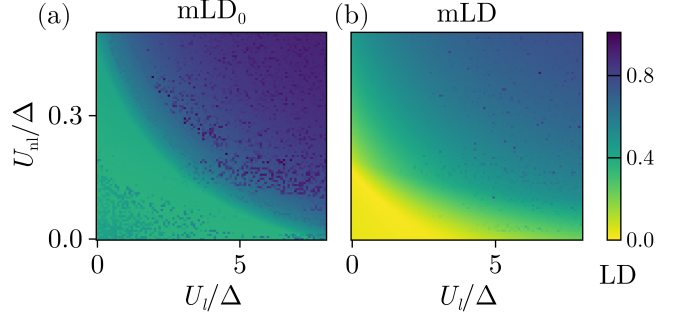


FIG. 8. LD at mLD_0 (a) and at mLD (b) as a function of the strength of local U_l and non-local U_{nl} Coulomb interaction. This is similar to the two-dot chain studied in Ref. [40]. The system can only tolerate a certain amount of interaction before strongly degrading the quality of the sweet spot.

Appendix C: Interactions

For the main conclusions of this article, we found that that interactions did not play a central role, and excluded them for simplicity. In Ref. [40], the role of interactions were studied in the two-dot system. There, the main conclusion was that if they are sufficiently small, they only slightly affect the quality of the sweet spot, while if they are too large, they may prohibit the tuning to the sweet spot. For the three-dot chain, we find qualitatively the same result, see Fig. 8. In Fig. 9 we show how the tuning plot changes when interactions are included.

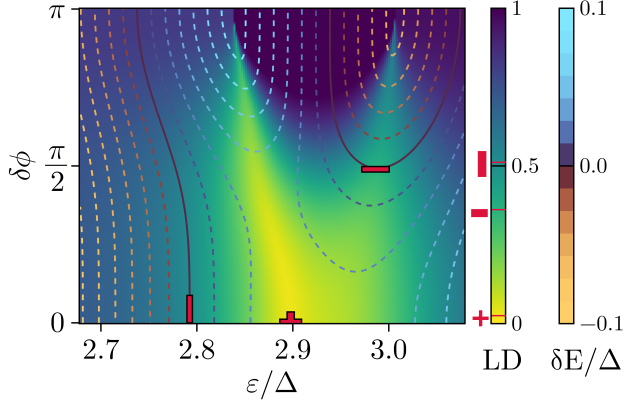


FIG. 9. LD as a function of $\delta\phi$ and ε . Same as Fig. 2 but with finite interactions where $U_l = 3\Delta$, $U_{nl} = \Delta/100$.

Appendix D: Effective Hamiltonian

In terms of the Bogoliubov quasiparticles where H_{QD} is diagonal, the Hamiltonians takes the form

$$H^{\text{QD}} = \sum_n \varepsilon_a a_n^\dagger a_n + \varepsilon_b b_n^\dagger b_n \quad (\text{D1})$$

$$H^C = \sum_n t_{aa} a_n^\dagger a_{n+1} + \Delta_{aa} a_n a_{n+1} + t_{ab} a_n^\dagger b_{n+1} + \Delta_{ab} a_n b_{n+1} - \Delta_{ba} a_{n+1} b_n + t_{ba} b_n^\dagger a_{n+1} + \Delta_{bb} b_n b_{n+1} + t_{bb} b_n^\dagger b_{n+1} + \text{h.c.}, \quad (\text{D2})$$

where

$$\varepsilon_a = \sqrt{\varepsilon^2 + \Delta^2} - V_Z \quad (\text{D3a})$$

$$\varepsilon_b = \sqrt{\varepsilon^2 + \Delta^2} + V_Z \quad (\text{D3b})$$

$$t_{aa} = -\frac{t\varepsilon \cos\left(\frac{\delta\phi}{2}\right)}{\sqrt{\Delta^2 + \varepsilon^2}} + it \sin\left(\frac{\delta\phi}{2}\right) \quad (\text{D3c})$$

$$t_{ab} = -\frac{\Delta t \cos\left(\frac{\delta\phi}{2}\right)}{\sqrt{\Delta^2 + \varepsilon^2}} \quad (\text{D3d})$$

$$\Delta_{aa} = -\frac{\Delta t_{\text{so}} \cos\left(\frac{\delta\phi}{2}\right)}{\sqrt{\Delta^2 + \varepsilon^2}} \quad (\text{D3e})$$

$$\Delta_{ab} = \frac{t_{\text{so}} \varepsilon \cos\left(\frac{\delta\phi}{2}\right)}{\sqrt{\Delta^2 + \varepsilon^2}} + it_{\text{so}} \sin\left(\frac{\delta\phi}{2}\right) \quad (\text{D3f})$$

$$t_{ba} = t_{ab} \quad (\text{D3g})$$

$$t_{bb} = t_{aa}^* \quad (\text{D3h})$$

$$\Delta_{bb} = -\Delta_{aa} \quad (\text{D3i})$$

$$\Delta_{ba} = \Delta_{ab}^* \quad (\text{D3j})$$

The first order term in the effective Hamiltonian is the projection onto states with no b -fermions,

$$H_1^{\text{eff}} = \sum_n \varepsilon_a a_n^\dagger a_n + (t_{aa} a_n^\dagger a_{n+1} + \Delta_{aa} a_n a_{n+1} + \text{h.c.}) \quad (\text{D4})$$

The second order term is

$$H_2^{\text{eff}} = \sum_n \varepsilon_2 a_n^\dagger a_n + t_2 a_n^\dagger a_{n+2} + \Delta_2 a_n^\dagger a_{n+2} + \text{h.c.} \quad (\text{D5})$$

where

$$\varepsilon_2 = 2(|\Delta_{ab}|^2 - |t_{ab}|^2)/\varepsilon_b \quad (\text{D6})$$

$$t_2 = (-\Delta_{ab}'^2 - t_{ab}^2)/\varepsilon_b \quad (\text{D7})$$

$$\Delta_2 = 2 \text{Re}\{\Delta_{ab} t_{ab}\}/\varepsilon_b \quad (\text{D8})$$

It includes the effect of next nearest neighbour hoppings and pairings.

Appendix E: Topological invariant

The topological invariant for the second order effective model (which is in class **D**) signifies when the gap closes at $k = 0$ or $k = \pi$ can be characterized by

$$Q \equiv \text{sign}(\text{Pf}(H_0) \text{Pf}(H_\pi)). \quad (\text{E1})$$

In the second order effective model, this is simply

$$Q \equiv \text{sign}((2 \text{Re}\{t_1 + t_2\} + \varepsilon)(2 \text{Re}\{-t_1 + t_2\} + \varepsilon)). \quad (\text{E2})$$

However, it should be noted that the gap can also close a finite momentum due to the breaking of time-reversal symmetry [68].

[1] A. Kitaev, Unpaired Majorana fermions in quantum wires, *Physics-Uspekhi* **44**, 131 (2001).

[2] J. Alicea, Y. Oreg, G. Refael, F. von Oppen, and M. P. A. Fisher, Non-Abelian statistics and topologi-

- cal quantum information processing in 1D wire networks, *Nature Physics* **7**, 412 (2011).
- [3] C. W. J. Beenakker, Search for non-Abelian Majorana braiding statistics in superconductors, *SciPost Physics Lecture Notes*, 15 (2020).
 - [4] J. Alicea, New directions in the pursuit of Majorana fermions in solid state systems, *Reports on Progress in Physics* **75**, 076501 (2012).
 - [5] M. Leijnse and K. Flensberg, Introduction to topological superconductivity and Majorana fermions, *Semiconductor Science and Technology* **27**, 124003 (2012).
 - [6] R. Aguado, Majorana quasiparticles in condensed matter, *La Rivista del Nuovo Cimento* **40**, 523 (2017).
 - [7] C. Nayak, S. H. Simon, A. Stern, M. Freedman, and S. D. Sarma, Non-Abelian Anyons and Topological Quantum Computation, *Reviews of Modern Physics* **80**, 1083 (2008).
 - [8] S. D. Sarma, M. Freedman, and C. Nayak, Majorana Zero Modes and Topological Quantum Computation, *npj Quantum Information* **1**, 15001 (2015).
 - [9] P. Marra, Majorana nanowires for topological quantum computation, *Journal of Applied Physics* **132**, 231101 (2022).
 - [10] Y. Oreg, G. Refael, and F. von Oppen, Helical Liquids and Majorana Bound States in Quantum Wires, *Physical Review Letters* **105**, 177002 (2010).
 - [11] R. M. Lutchyn, J. D. Sau, and S. D. Sarma, Majorana Fermions and a Topological Phase Transition in Semiconductor-Superconductor Heterostructures, *Physical Review Letters* **105**, 077001 (2010).
 - [12] S. Vaitiekėnas, G. W. Winkler, B. van Heck, T. Karzig, M.-T. Deng, K. Flensberg, L. I. Glazman, C. Nayak, P. Krogstrup, R. M. Lutchyn, and C. M. Marcus, Flux-induced topological superconductivity in full-shell nanowires, *Science* **367**, eaav3392 (2020).
 - [13] V. Mourik, K. Zuo, S. M. Frolov, S. R. Plissard, E. P. A. M. Bakkers, and L. P. Kouwenhoven, Signatures of Majorana Fermions in Hybrid Superconductor-Semiconductor Nanowire Devices, *Science* **336**, 1003 (2012).
 - [14] A. Das, Y. Ronen, Y. Most, Y. Oreg, M. Heiblum, and H. Shtrikman, Zero-bias peaks and splitting in an Al-InAs nanowire topological superconductor as a signature of Majorana fermions, *Nature Physics* **8**, 887 (2012).
 - [15] M. T. Deng, S. Vaitiekėnas, E. B. Hansen, J. Danon, M. Leijnse, K. Flensberg, J. Nygård, P. Krogstrup, and C. M. Marcus, Majorana bound state in a coupled quantum-dot hybrid-nanowire system, *Science* **354**, 1557 (2016).
 - [16] S. Nadj-Perge, I. K. Drozdov, B. A. Bernevig, and A. Yazdani, Proposal for realizing Majorana fermions in chains of magnetic atoms on a superconductor, *Physical Review B* **88**, 020407 (2013).
 - [17] S. Nadj-Perge, I. K. Drozdov, J. Li, H. Chen, S. Jeon, J. Seo, A. H. MacDonald, B. A. Bernevig, and A. Yazdani, Observation of Majorana fermions in ferromagnetic atomic chains on a superconductor, *Science* **346**, 602 (2014).
 - [18] F. Pientka, A. Keselman, E. Berg, A. Yacoby, A. Stern, and B. I. Halperin, Topological Superconductivity in a Planar Josephson Junction, *Physical Review X* **7**, 021032 (2017).
 - [19] M. Hell, M. Leijnse, and K. Flensberg, Two-Dimensional Platform for Networks of Majorana Bound States, *Physical Review Letters* **118**, 107701 (2017).
 - [20] A. Fornieri, A. M. Whiticar, F. Setiawan, E. Portolés, A. C. C. Drachmann, A. Keselman, S. Gronin, C. Thomas, T. Wang, R. Kallagher, G. C. Gardner, E. Berg, M. J. Manfra, A. Stern, C. M. Marcus, and F. Nichele, Evidence of topological superconductivity in planar Josephson junctions, *Nature* **569**, 89 (2019).
 - [21] H. Ren, F. Pientka, S. Hart, A. T. Pierce, M. Kosowsky, L. Lunczer, R. Schlereth, B. Scharf, E. M. Hankiewicz, L. W. Molenkamp, B. I. Halperin, and A. Yacoby, Topological superconductivity in a phase-controlled Josephson junction, *Nature* **569**, 93 (2019).
 - [22] G. Kells, D. Meidan, and P. W. Brouwer, Near-zero-energy end states in topologically trivial spin-orbit coupled superconducting nanowires with a smooth confinement, *Physical Review B* **86**, 100503 (2012).
 - [23] E. Prada, P. San-Jose, and R. Aguado, Transport spectroscopy of NS nanowire junctions with Majorana fermions, *Physical Review B* **86**, 180503 (2012).
 - [24] J. Liu, A. C. Potter, K. T. Law, and P. A. Lee, Zero-Bias Peaks in the Tunneling Conductance of Spin-Orbit-Coupled Superconducting Wires with and without Majorana End-States, *Physical Review Letters* **109**, 267002 (2012).
 - [25] D. Roy, N. Bondyopadhyaya, and S. Tewari, Topologically trivial zero-bias conductance peak in semiconductor Majorana wires from boundary effects, *Physical Review B* **88**, 020502 (2013).
 - [26] C.-X. Liu, J. D. Sau, T. D. Stanescu, and S. Das Sarma, Andreev bound states versus Majorana bound states in quantum dot-nanowire-superconductor hybrid structures: Trivial versus topological zero-bias conductance peaks, *Physical Review B* **96**, 075161 (2017).
 - [27] C. Moore, C. Zeng, T. D. Stanescu, and S. Tewari, Quantized zero-bias conductance plateau in semiconductor-superconductor heterostructures without topological Majorana zero modes, *Physical Review B* **98**, 155314 (2018).
 - [28] C. Reeg, O. Dmytruk, D. Chevallier, D. Loss, and J. Klinovaja, Zero-energy Andreev bound states from quantum dots in proximitized Rashba nanowires, *Physical Review B* **98**, 245407 (2018).
 - [29] O. A. Awoga, J. Cayao, and A. M. Black-Schaffer, Super-current Detection of Topologically Trivial Zero-Energy States in Nanowire Junctions, *Physical Review Letters* **123**, 117001 (2019).
 - [30] A. Vuik, B. Nijholt, A. R. Akhmerov, and M. Wimmer, Reproducing topological properties with quasi-Majorana states, *SciPost Physics* **7**, 061 (2019).
 - [31] H. Pan and S. Das Sarma, Physical mechanisms for zero-bias conductance peaks in Majorana nanowires, *Physical Review Research* **2**, 013377 (2020).
 - [32] E. Prada, P. San-Jose, M. W. A. de Moor, A. Geresdi, E. J. H. Lee, J. Klinovaja, D. Loss, J. Nygård, R. Aguado, and L. P. Kouwenhoven, From Andreev to Majorana bound states in hybrid superconductor-semiconductor nanowires, *Nature Reviews Physics* **2**, 575 (2020).
 - [33] R. Hess, H. F. Legg, D. Loss, and J. Klinovaja, Local and nonlocal quantum transport due to Andreev bound states in finite Rashba nanowires with superconducting and normal sections, *Physical Review B* **104**, 075405 (2021).
 - [34] J. D. Sau and S. D. Sarma, Realizing a robust practical Majorana chain in a quantum-dot-superconductor linear array, *Nature Communications* **3**, 964 (2012).

- [35] M. Leijnse and K. Flensberg, Parity qubits and poor man's Majorana bound states in double quantum dots, *Physical Review B* **86**, 134528 (2012).
- [36] I. C. Fulga, A. Haim, A. R. Akhmerov, and Y. Oreg, Adaptive tuning of Majorana fermions in a quantum dot chain, *New Journal of Physics* **15**, 045020 (2013).
- [37] C.-X. Liu, G. Wang, T. Dvir, and M. Wimmer, Tunable Superconducting Coupling of Quantum Dots via Andreev Bound States in Semiconductor-Superconductor Nanowires, *Physical Review Letters* **129**, 267701 (2022).
- [38] A. Tsintzis, R. S. Souto, and M. Leijnse, Creating and detecting poor man's Majorana bound states in interacting quantum dots, *Physical Review B* **106**, L201404 (2022).
- [39] C.-X. Liu, A. M. Bozkurt, F. Zatelli, S. L. D. ten Haaf, T. Dvir, and M. Wimmer, Enhancing the excitation gap of a quantum-dot-based Kitaev chain, *Communications Physics* **7**, 1 (2024).
- [40] W. Samuelson, V. Svensson, and M. Leijnse, Minimal quantum dot based Kitaev chain with only local superconducting proximity effect, *Physical Review B* **109**, 035415 (2024).
- [41] J. D. T. Luna, A. M. Bozkurt, M. Wimmer, and C.-X. Liu, Flux-tunable Kitaev chain in a quantum dot array (2024), arXiv:2402.07575 [cond-mat].
- [42] G. Wang, T. Dvir, G. P. Mazur, C.-X. Liu, N. van Loo, S. L. D. ten Haaf, A. Bordin, S. Gazibegovic, G. Badawy, E. P. A. M. Bakkers, M. Wimmer, and L. P. Kouwenhoven, Singlet and triplet Cooper pair splitting in hybrid superconducting nanowires, *Nature* **612**, 448 (2022).
- [43] T. Dvir, G. Wang, N. van Loo, C.-X. Liu, G. P. Mazur, A. Bordin, S. L. D. ten Haaf, J.-Y. Wang, D. van Driel, F. Zatelli, X. Li, F. K. Malinowski, S. Gazibegovic, G. Badawy, E. P. A. M. Bakkers, M. Wimmer, and L. P. Kouwenhoven, Realization of a minimal Kitaev chain in coupled quantum dots, *Nature* **614**, 445 (2023).
- [44] F. Zatelli, D. van Driel, D. Xu, G. Wang, C.-X. Liu, A. Bordin, B. Roovers, G. P. Mazur, N. van Loo, J. C. Wolff, A. M. Bozkurt, G. Badawy, S. Gazibegovic, E. P. A. M. Bakkers, M. Wimmer, L. P. Kouwenhoven, and T. Dvir, Robust poor man's Majorana zero modes using Yu-Shiba-Rusinov states, *Nature Communications* **15**, 7933 (2024).
- [45] S. L. D. ten Haaf, Q. Wang, A. M. Bozkurt, C.-X. Liu, I. Kulesh, P. Kim, D. Xiao, C. Thomas, M. J. Manfra, T. Dvir, M. Wimmer, and S. Goswami, A two-site Kitaev chain in a two-dimensional electron gas, *Nature* **630**, 329 (2024).
- [46] R. S. Souto, A. Tsintzis, M. Leijnse, and J. Danon, Probing Majorana localization in minimal Kitaev chains through a quantum dot, *Physical Review Research* **5**, 043182 (2023).
- [47] C.-X. Liu, H. Pan, F. Setiawan, M. Wimmer, and J. D. Sau, Fusion protocol for Majorana modes in coupled quantum dots, *Physical Review B* **108**, 085437 (2023).
- [48] P. Boross and A. Pályi, Braiding-based quantum control of a Majorana qubit built from quantum dots, *Physical Review B* **109**, 125410 (2024).
- [49] A. Tsintzis, R. S. Souto, K. Flensberg, J. Danon, and M. Leijnse, Majorana Qubits and Non-Abelian Physics in Quantum Dot-Based Minimal Kitaev Chains, *PRX Quantum* **5**, 010323 (2024).
- [50] N. Sedlmayr and C. Bena, Visualising Majorana bound states in 1D and 2D using the generalized Majorana polarization, *Physical Review B* **92**, 115115 (2015).
- [51] N. Sedlmayr, J. M. Aguiar-Hualde, and C. Bena, Majorana bound states in open quasi-1D and 2D systems with transverse Rashba coupling, *Physical Review B* **93**, 155425 (2016).
- [52] S. V. Aksenov, A. O. Zlotnikov, and M. S. Shustin, Strong Coulomb interactions in the problem of Majorana modes in a wire of the nontrivial topological class BDI, *Physical Review B* **101**, 125431 (2020).
- [53] E. M. Stoudenmire, J. Alicea, O. A. Starykh, and M. P. A. Fisher, Interaction Effects in Topological Superconducting Wires Supporting Majorana Fermions, *Physical Review B* **84**, 014503 (2011).
- [54] A. R. Wright and M. Veldhorst, Localized Many-Particle Majorana Modes with Vanishing Time-Reversal Symmetry Breaking in Double Quantum Dots, *Physical Review Letters* **111**, 096801 (2013).
- [55] T. E. O'Brien, A. R. Wright, and M. Veldhorst, Many-particle Majorana bound states: Derivation and signatures in superconducting double quantum dots, *physica status solidi (b)* **252**, 1731 (2015).
- [56] T. E. O'Brien and A. R. Wright, A many-body interpretation of Majorana bound states, and conditions for their localisation (2015), arXiv:1508.06638 [cond-mat].
- [57] G. Kells, Many-body Majorana operators and the equivalence of parity sectors, *Physical Review B* **92**, 081401 (2015).
- [58] G. Kells, Multiparticle content of Majorana zero modes in the interacting p-wave wire, *Physical Review B* **92**, 155434 (2015).
- [59] A. M. Bozkurt, S. Miles, S. L. D. ten Haaf, C.-X. Liu, F. Hassler, and M. Wimmer, Interaction-induced strong zero modes in short quantum dot chains with time-reversal symmetry (2024), arXiv:2405.14940 [cond-mat].
- [60] A. Bordin, X. Li, D. van Driel, J. C. Wolff, Q. Wang, S. L. D. ten Haaf, G. Wang, N. van Loo, L. P. Kouwenhoven, and T. Dvir, Crossed Andreev reflection and elastic co-tunneling in a three-site Kitaev chain nanowire device (2023), arXiv:2306.07696 [cond-mat].
- [61] A. Bordin, C.-X. Liu, T. Dvir, F. Zatelli, S. L. D. ten Haaf, D. van Driel, G. Wang, N. van Loo, T. van Caekenberghe, J. C. Wolff, Y. Zhang, G. Badawy, S. Gazibegovic, E. P. A. M. Bakkers, M. Wimmer, L. P. Kouwenhoven, and G. P. Mazur, Signatures of Majorana protection in a three-site Kitaev chain (2024), arXiv:2402.19382 [cond-mat].
- [62] C.-X. Liu, S. Miles, A. Bordin, S. L. D. ten Haaf, A. M. Bozkurt, and M. Wimmer, Protocol for scaling up a sign-ordered Kitaev chain without magnetic flux control (2024), arXiv:2407.04630 [cond-mat].
- [63] M. Ezawa, Even-odd effect on robustness of Majorana edge states in short Kitaev chains, *Physical Review B* **109**, L161404 (2024).
- [64] In the full model, there are two fermions on each site because there are two spins. In the effective model, see Sec. IV B, there is only one.
- [65] Different bounds result from using Hölder's inequality $|\text{Tr}[\mathcal{O}_R \delta \rho]| \leq \|\mathcal{O}_R\|_q \|\delta \rho_R\|_p$, where $1/q + 1/p = 1$ and $\|\cdot\|_q$ is the Schatten norm. Without additional assumptions on the perturbation, we have no reason to prefer one over another.
- [66] V. Svensson, Cvsvensson/LongerPoorMansMajoranas (2024).

- [67] S. Miles, D. van Driel, M. Wimmer, and C.-X. Liu, Kitaev chain in an alternating quantum dot-Andreev bound state array, *Physical Review B* **110**, 024520 (2024).
- [68] W. DeGottardi, M. Thakurathi, S. Vishveshwara, and D. Sen, Majorana fermions in superconducting wires: Effects of long-range hopping, broken time-reversal symmetry, and potential landscapes, *Physical Review B* **88**, 165111 (2013).
- [69] A. Alecce and L. Dell’Anna, Extended Kitaev chain with longer-range hopping and pairing, *Physical Review B* **95**, 195160 (2017).
- [70] I. Mahyaeh and E. Ardonne, Zero modes of the Kitaev chain with phase-gradients and longer range couplings, *Journal of Physics Communications* **2**, 045010 (2018).
- [71] M.-C. Chung and I. Peschel, Density-matrix spectra of solvable fermionic systems, *Physical Review B* **64**, 064412 (2001).
- [72] S.-A. Cheong and C. L. Henley, Many-body density matrices for free fermions, *Physical Review B* **69**, 075111 (2004).